Optics Letters

Interferometry-free noncontact photoacoustic detection method based on speckle correlation change

Huanhao Li,[1,2] Fei Cao,[1,2] Yingying Zhou,[1,2] Zhipeng Yu,[1,2] and Puxiang Lai[1,2,*]

[1]Department of Biomedical Engineering, The Hong Kong Polytechnic University, Hong Kong SAR, China
[2]The Hong Kong Polytechnic University Shenzhen Research Institute, Shenzhen, China
*Corresponding author: puxiang.lai@polyu.edu.hk

Received 10 September 2019; revised 8 October 2019; accepted 9 October 2019; posted 14 October 2019 (Doc. ID 377132); published 8 November 2019

Optical speckle patterns occur when a coherent optical wavefront is randomized but such stochastic yet deterministic information about the medium can be decoded. A simple setup is inspired to monitor the decorrelation of speckle patterns within the memory effect range when the medium is photoacoustically perturbated. Experimentally, a linear relationship is confirmed between the speckle correlation change and the peak-to-peak amplitude of the ultrasonic transducer-detected photoacoustic waves, and the detection sensitivity is comparable. Such a plain specklegram-based method may find special interests when no direct contact is allowed between the sample and the photoacoustic detector.

https://doi.org/10.1364/OL.44.005481

Optical scattering randomizes the propagation of light, and it occurs almost universally due to the presence of rough surfaces and/or inhomogeneities of the refractive index for most of the artifacts or substances in nature. A randomized coherent optical wavefront leads to random interferences or optical speckle patterns. These seemingly random yet deterministic patterns can be very sensitive to perturbations acted upon the medium. By scrutinizing these speckle patterns, various types of information can be extracted: for example, imaging blood flow beneath the skin via the contrast of speckle patterns [1], and visualizing a hidden object by analyzing the spatial correlation among speckle patterns [2] and a wavemeter [3,4]. Moreover, by actively shaping the incident wavefront, image transmission [5,6] and optical focusing [7–11] through/inside a complex medium can be achieved. Therefore, decoding the specklegram allows one to remotely characterize the physical status of the interacting medium as well as its response to small perturbations, potentially benefiting scenarios where direct contact is inhibited between the medium and the sensor.

All-optical noncontact photoacoustic detection poses one such scene. In photoacoustics (PA), light is absorbed by the medium and converted into heat that leads to thermal expansion, generating ultrasonic waves. These photoacoustic waves are scattered much less than light is in biological tissues, thus are able to propagate within tissue without substantial loss. Moreover, substances of distinct optical absorption spectra can define high optical contrast in tissues via proper wavelength selection. Photoacoustic imaging has seen extensive investigations [12]. In most of these studies, piezoelectric (PZT) transducers are the very choice for receiving the PA waves. These transducers allow manufacturing of arrays with many detectors along with promising performance regarding resolution, sensitivity, and well-defined central frequency. The ultrasound-induced perturbations can be optically probed with proper coupling strategy without a piezoelectric transducer (PZT). For instance, differentiated reflectances of two polarized beams can identify the small ultrasonic perturbations [13,14]. These contact-based approaches, including a PZT, need a coupling medium (e.g., water), posing limited capabilities in some inspection or clinical scenarios where dehydrated condition is desired. To address this dilemma, noncontact PA detection is called for. One of the representative realizations is using an optical beam (probe beam) reflected or backscattered from the sample disturbed by the PA waves. To demodulate the PA information encoded in the probe beam, another optical beam (reference beam) is introduced to interfere with the probe beam [15,16]. With this interferometer, the strengths of the ultrasonic-induced perturbations to the sample, such as phase variations, can be deciphered, say, being converted into proportional intensity modulations [17,18].

While promising, wide application of such an interferometry-based scheme is hindered by the need for the reference beam, which complicates the system. A recent study sheds light on the possibility for noncontact via a confocal setup, using a low-coherence light source to reject phase modulation from the sample [19,20]. Nevertheless, phase modulation itself is still valuable to learn about the perturbations. In this work, we introduce a new noncontact PA detection approach through decoding the specklegram nature of the probe beam only; no reference beam is involved herein since the specklegram itself inherently contains interference information spatiotemporally.

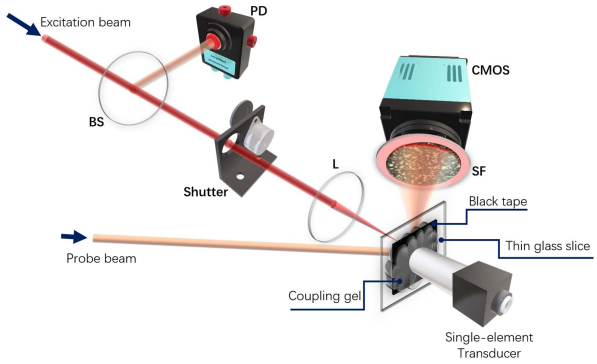

Fig. 1. Schematic setup for specklegram-based noncontact photoacoustic detection. BS, beamsplitter; CMOS, CMOS camera; L, lens; PD, photodiode; SF, spectral filter.

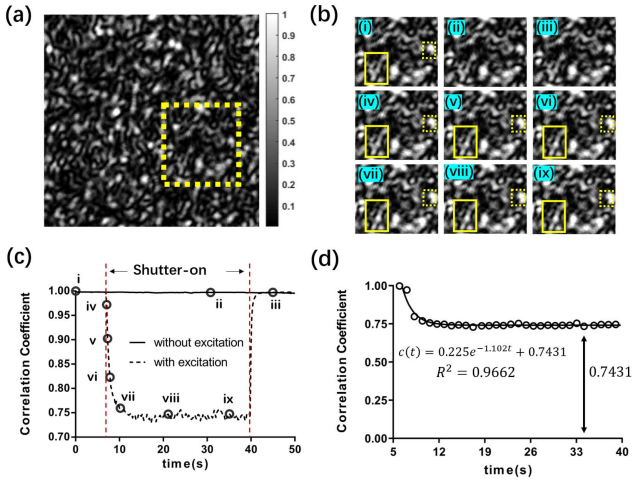

Fig. 2. Observation and quantification of photoacoustically perturbated speckle pattern. (a) A speckle pattern generated by the probe beam. The highlighted region (dashed rectangle) is zoomed in for analysis. (b) Representative zoomed-in observations for various moments (i)–(ix) in (c). Among them, (i) is the initial speckle pattern, (ii) and (iii) are recorded when the shutter is off and no excitation beam illuminated on the sample, and (iv)–(ix) are a sequence of patterns associated with the excitation of PA effect. (c) Correlation coefficients of the speckle patterns as a function of time. Shutter-on implies the triggering of the PA excitation. (d) The strength of the PA perturbations is quantified by the reduction of the correlation coefficient, i.e., the speckle correlation change (SCC).

Only one CMOS camera is needed to record the speckle patterns of the probe beam reflected and backscattered from the medium, and no demanding optical alignment is necessary. In the presence of photoacoustic perturbations, the refractive index and scatters within the medium are shifted, affecting the propagation of the probe beam and causing changes to the speckle patterns. Hence, the photoacoustic perturbation information, such as the strength, is coupled into the variations of the recorded specklegram. For simplicity, in this work photoacoustic perturbations are relatively small and fall within the "memory effect regime" [21] so that the speckle correlation change (SCC) is linearly or approximately linearly associated with the strength of the PA effect.

The system is shown in Fig. 1, with two optical beams: an excitation beam and a probe beam. The excitation beam is from a pulse optical parametric oscillator laser (NT230, EKSPLA, UK) with a wavelength of 740 nm and a repetition rate of 100 Hz, and it is focused onto the sample surface to generate PA signals. The probe beam is from a 650 nm continuous-wave laser (HW650AD30-12GD, Shenzhen Near Infrared Laser, China), illuminating onto the surface of the investigated sample obliquely so that the reflected and backscattered light forms speckle patterns. These patterns are monitored by a CMOS camera (FL3-U3-32S2M-CS, Pointgrey, Canada) at 60 Hz, with 10 μs exposure time to ensure each exposure contains only one pulse from the excitation beam. An optical spectral filter of 650 nm is mounted on the camera to prevent the 740 nm light from affecting the probed speckle pattern. During experiment, the intensity of excitation beam is adjusted by a tunable attenuator (not shown in Fig. 1) to tune the strength of the PA signal. The excitation beam is divided into two paths by a 10/90 beamsplitter to create an optical path for a photodiode (PDA36A-EC, Thorlabs, USA), which is used to normalize the pulse-to-pulse intensity fluctuations of the excitation beam. For simplicity, a black tape of 150 μm thickness and 15 mm × 15 mm area is adhered to a 170-μm-thick glass slice as the experimental sample. For verification and comparison purpose, a 10 MHz PZT (NDT V327-SU-F0.60IN-PTF, Olympus, Japan) is also configured to receive the PA signals, which are amplified by a preamplifier (ZFL-500LN-BNC+, Mini-Circuits, USA) and then digitized by an oscilloscope (DS4024, RIGOL, USA). To control the presence of the excitation beam, and hence the PA perturbation, before the sample, a fast-electronic shutter (USB optical shutter, Picard Industries, USA) is mounted. The OPO laser, the photodiode, the shutter, and the CMOS camera are synchronized and controlled via MATLAB.

The CMOS-captured speckle patterns were screened, beginning from an initial stable speckle pattern (I_0) in the absence of the PA effect to the following photoacoustically perturbated patterns (I_t). As shown in Fig. 2(a), the speckle grains are erratically distributed in space, and the PA-induced perturbations are encoded in such a seemingly random pattern. It is unrealistic and labor-consuming to study the variations of all individual speckle grains. Moreover, the individual grains may contribute differently to the overall ensembled pattern. Therefore, speckles and their variations are usually analyzed statistically [22], and so is this study. A Pearson's correlation coefficient is used to characterize the speckle temporal correlation as follows:

$$c(t) = \frac{\langle (I_0 - \langle I_0 \rangle)(I_t - \langle I_t \rangle) \rangle}{\sigma_0 \sigma_t}.$$

A sequence of speckle patterns is recorded before and after the PA perturbation is induced, with some representative patterns shown in Fig. 2(b). In the first group, (i) is the initial speckle pattern (I_0), and (ii) and (iii) are sampled when the shutter remains closed. In the second group, (iv)–(ix) are sampled in sequence after the shutter is opened and the PA perturbations are induced. Note that the morphological differences among these samples are slight, but these variations can be clearly seen statistically. In Fig. 2(c), the correlation coefficient for all speckle patterns with respect to the initial one is shown as a function of time. As seen, in the absence of PA excitation

(shutter is closed to block the excitation beam), the speckle correlation coefficient decays imperceptibly over time, suggesting the experimental system is reliably stable for small perturbation detection. Note that generally other factors such as environmental noise or system instability may also affect the specklegram. This, however, does not affect the results in this study: the speckle correlation decays very slowly in the absence of the PA effect, suggesting a very stable optical system; the reduction from and the recovery back to the stability curve is solely related to the on and off of the excitation beam.

However, when the shutter is opened, the speckle grains begin to evolve, albeit subtly, due to the PA perturbations. The correlation curve magnifies the seemingly tiny variations. The correlation coefficient drops quickly from 1 to 0.742, reaching plateaus with small fluctuations due to the continuing PA perturbations. When the shutter is turned off and the excitation beam is blocked again [$t \approx 40$ s in the Fig. 2(c)], the correlation coefficient bounces rapidly back to its initial state close to unity as there is no more perturbation. In this study, the abovementioned plateau is used to be correlated to the strength of the corresponding PA perturbation, as illustrated in Fig. 2(d). A negative exponential model with parameters (α, β, γ), $c(t) = \alpha e^{-\beta t} + \gamma$ is used to fit the correlation curve when the PA excitation beam is unblocked. The value of γ is related to the strength of the perturbation when the speckles are stabilized again under continuing perturbations. Therefore, the SCC, defined by $\Delta c = 1 - \gamma$, can be used for characterizing the strength of the excited PA signals.

To investigate how the SCC is affected by the intensity of the excitation beam, the optical fluence of the excitation beam is gradually tuned from 0 to 0.0048 mJ/cm^2. Following the protocol discussed above, all corresponding speckle patterns are recorded and analyzed. A few representative temporal correlation curves are shown in Fig. 3(a). As seen, varying the excitation beam intensity does not alter the shape of the correlation curve drastically, but stronger excitation does deepen the plateau of the curves. It suggests that stronger PA perturbation varies the speckle patterns more, leading to a lower correlation coefficient, and hence a larger SCC and lower C(t). The PA signal (optical energy = 0.0045 mJ/cm^2) detected by PZT is also shown in Fig. 3(d), which is temporally synchronized with Fig. 3(a). The PA signal is characterized by the peak–peak difference of the waveform indicated in the inset of Fig. 3(d), and it is denoted as PA(t).

When the state of the shutter is altered, i.e., at the beginning (time window: 6–15 s) and the end (time window: 39.5–42.0 s) of the shutter period, $C(t)$ and PA(t) perform quite differently: a rapid response detected by the PZT (standard photoacoustic detection methods) and a much slower response captured by the camera (the optical speckle pattern of the reflected probe beam). Considering the framerate of the camera used in the study is 100 Hz (corresponding to a 10 ms scale intermediate process), the prolonged transition periods of the speckle correlations should be attributed to the spreading of heat. In the current setup, the probe beam is nonfocused at the sample interface, and thus the reflected speckle pattern is sensitive to motions of the sample surface within a relatively large region. In the experiment, as the heat gradually spreads out, which is on the timescale of seconds [23], more and more surficial regions are disturbed and contribute to the decorrelation of the speckle patterns. After a few seconds, when the heat spreading and dissipation reach an equilibrium, the SCC curve sees a plateau [Fig. 3(b)]. Similarly, when the shutter is off, the PA signal as detected by the PZT disappears instantly and only background noise is left [Fig. 3(d)], but as the heat needs some time to dissipate, it takes ~2 s for the correlation coefficient to go back to one [Fig. 3(c)].

Despite the temporal mismatch between the PZT detection and the SCC due to mechanism variation, the SCC can still be used to measure the strength of the PA signals. In Fig. 4(a) (right axis), the resultant SCC is plotted against the excitation beam pulse energy. As seen, once the excitation beam is beyond a threshold (~0.002792 mJ/cm^2), the SCC increases almost linearly ($R^2 = 0.9106$) with the excitation beam energy. The trend is quite similar to Fig. 4(a) (left axis), where the PZT-detected PA signal also increases linearly with the pulse energy once it is beyond a threshold. More importantly, it is one-to-one mapped between the two methods of detection in response to same optical excitation, as shown in Fig. 4(b). It is thus confirmed that the proposed speckle correlation change (Δc) is linearly proportional to the strength of PA perturbations. On the other hand, if we further examine the two excitation thresholds before linearity dominates in Fig. 4(a), we can see both are

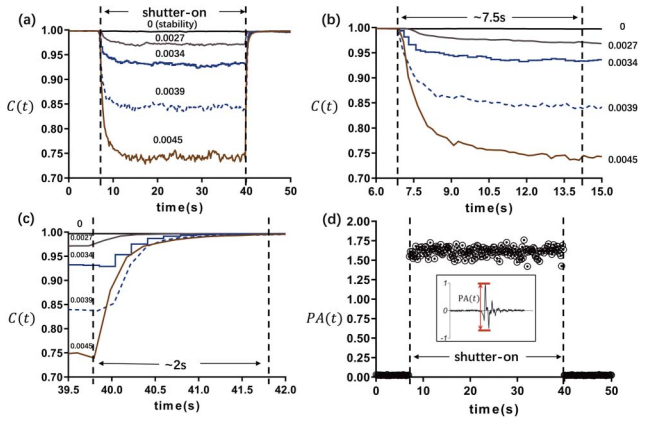

Fig. 3. Photoacoustic detection based on the proposed specklegram method and the standard PZT method. (a) A few representative temporal correlation curves with different excitation beam pulse energies. (b–c) Zoom-in representations from (a) between $t = 6$–15 s and 39.5–42.0 s, respectively. (d) Instant PA amplitude as a function of time, as extracted from the peak-to-peak values of PZT-detected waveforms (the inset). The optical fluences are denoted beside the corresponding curves in mJ/cm^2.

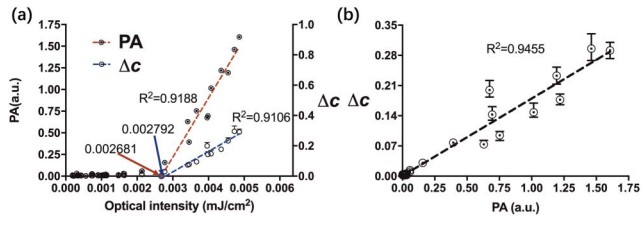

Fig. 4. (a) Measured SCC as a function of excitation pulse energy (right axis) and the PZT-based PA amplitude as a function of excitation pulse energy (left axis). (b) Linearity between the two detection methods. Error bars in (a) and (b) are the standard deviation of Δc extracted from the measurements.

quite close (0.002792 and 0.002681 mJ/cm^2, respectively), suggesting comparable detection sensitivity.

Before concluding, a few clarifications are needed here. The perturbation to the speckle pattern may contain different frequency components, whose weighted sum results in the reported observation — the encoded envelope of the broadband PA signals — due to the finite exposure time and frame rate of the camera. The PA signals hereby are detected by a 10 MHz focused ultrasonic transducer as the reference and gold standard. The results indicate that at least the proposed speckle decorrelation can characterize the strength of 10 MHz PA signals. To further quantify the frequency range, however, it may need a complicated mathematical model, which is beyond the scope of the current paper and might be explored in future work. Nevertheless, the proposed scheme provides an interferometry-free and noncontact intervention to detect the strength of PA effects. The detection setup is rather plain, merely containing a probing laser to generate speckle patterns and a digital camera to capture the specklegrams; there is no strict requirement for optical alignment. And the camera can be replaced by many commercial cameras or even the camera of modern cell phones. However, it must be pointed out, the limited frame rate of the camera-based detection paralyzes the capability of resolving the temporal profile of PA signals along the acoustic axis; the observed decorrelation of speckle patterns is an integrated accumulation rather than a "point" sensing. This sets a major drawback of the proposed method.

Lastly but not the least, typically when the correlation coefficient drops lower than $e^{-1} \approx 0.3679$ the speckle pattern is regarded as being decorrelated and visually identified as another speckle pattern that is statistically different from the original one [21]. In this study, the minimum correlation coefficient is 0.7431 [Fig. 3(a)], indicating that the perturbated speckle patterns, although experiencing decorrelations, are still correlated within the memory effect regime. It also suggests that the refractive index variation of the sample is tiny due to the PA-induced vibrations and thermal effect. The main features of the speckle grains are thereby retained, as observed in Fig. 2(b). Taking the advantages of the memory effect, we thus can relate speckle variations linearly or quasi-linearly to the small perturbations applied onto the sample. Therefore, we can decouple the encoded PA (envelope) signal strength from the SCC linearly in this study. Of course, if a stronger PA effect is generated, the detected SCC may exceed e^{-1} and hence can no longer be used to delineate the PA signal strength.

Collectively, the study is built upon that fact that speckle patterns contain rich information, and it is very sensitive to medium motion. The hypothesis is, therefore, whether we can exploit the speckle changes to detect small perturbations induced by the PA effect. The feasibility has been demonstrated experimentally in this study, showing the correlation of speckle patterns can be used to delineate the strength of PA signals (as measured by the gold standard method). Such a plain specklegram-based method may find special interests for applications where no direct contact is allowed between the sample and the photoacoustic detector. Moreover, unlike other noncontact PA detection methods that have been reported, no optical interferometer is needed; the forming of speckle patterns itself serves as a delicate scheme to demodulate photoacoustically encoded information. The next phase will combine new schemes, such as compressed ultrafast photography [24–26], to exceed the current bandwidth barrier, aiming at more applications.

Funding. National Natural Science Foundation of China (81627805, 81671726, 81930048); Hong Kong Research Grant Council (25204416); Hong Kong Innovation and Technology Commission (ITS/022/18); Shenzhen Science and Technology Innovation Commission (JCYJ20170818104421564).

Disclosures. The authors declare no conflicts of interest.

REFERENCES

1. D. A. Boas and A. K. Dunn, J. Biomed. Opt. **15**, 011109 (2010).
2. O. Katz, P. Heidmann, M. Fink, and S. Gigan, Nat. Photonics **8**, 784 (2014).
3. B. Redding, S. F. Liew, R. Sarma, and H. Cao, Nat. Photonics **7**, 746 (2013).
4. G. D. Bruce, L. O'Donnell, M. Chen, and K. Dholakia, Opt. Lett. **44**, 1367 (2019).
5. S. Popoff, G. Lerosey, M. Fink, A. C. Boccara, and S. Gigan, Nat. Commun. **1**, 81 (2010).
6. Z. Yaqoob, D. Psaltis, M. S. Feld, and C. Yang, Nat. Photonics **2**, 110 (2008).
7. I. M. Vellekoop and A. Mosk, Opt. Lett. **32**, 2309 (2007).
8. J. Yang, Y. Shen, Y. Liu, A. S. Hemphill, and L. V. Wang, Appl. Phys. Lett. **111**, 201108 (2017).
9. Z. Yu, H. Li, and P. Lai, Appl. Sci. **7**, 1320 (2017).
10. P. Lai, L. Wang, J. W. Tay, and L. V. Wang, Nat. Photonics **9**, 126 (2015).
11. Y. Liu, P. Lai, C. Ma, X. Xu, A. A. Grabar, and L. V. Wang, Nat. Commun. **6**, 5904 (2015).
12. L. V. Wang and S. Hu, Science **335**, 1458 (2012).
13. F. Yang, W. Song, C. Zhang, C. Min, H. Fang, L. Du, P. Wu, W. Zheng, C. Li, S. Zhu, and X. Yuan, Nanoscale **10**, 8606 (2018).
14. X. Zhu, Z. Huang, G. Wang, W. Li, D. Zou, and C. Li, Opt. Lett. **42**, 439 (2017).
15. G. Rousseau, B. Gauthier, A. Blouin, and J. P. Monchalin, J. Biomed. Opt. **17**, 061217 (2012).
16. C. Buj, J. Horstmann, M. Münter, and R. Brinkmann, *Current Directions in Biomedical Engineering* (2015), Vol. **1**.
17. P. Lai, J. R. McLaughlan, A. B. Draudt, T. W. Murray, R. O. Cleveland, and R. A. Roy, Ultrasound Med. Biol. **37**, 239 (2011).
18. F. Ramaz, B. Forget, M. Atlan, A. C. Boccara, M. Gross, P. Delaye, and G. Roosen, Opt. Express **12**, 5469 (2004).
19. P. Hajireza, W. Shi, K. Bell, R. J. Paproski, and R. J. Zemp, Light Sci. Appl. **6**, e16278 (2017).
20. K. Bell, P. Hajireza, and R. Zemp, Opt. Lett. **43**, 146 (2018).
21. I. Freund, M. Rosenbluh, and S. Feng, Phys. Rev. Lett. **61**, 2328 (1988).
22. J. W. Goodman, *Speckle Phenomena in Optics: Theory and Applications* (Roberts and Company, 2007).
23. A. Vakili, J. L. Hollmann, R. G. Holt, and C. A. DiMarzio, J. Biomed. Opt. **22**, 106004 (2017).
24. X. L. Liu, J. D. Liu, C. Jiang, F. Vetrone, and J. Y. Liang, Opt. Lett. **44**, 1387 (2019).
25. L. Gao, J. Y. Liang, C. Y. Li, and L. H. V. Wang, Nature **516**, 74 (2014).
26. Y. Lu, T. T. W. Wong, F. Chen, and L. D. Wang, Phys. Rev. Lett. **122**, 193904 (2019).